Hindawi
Advances in Civil Engineering
Volume 2023, Article ID 8288308, 13 pages
https://doi.org/10.1155/2023/8288308

Research Article

Nonlinear Behavior Study of Reinforced Concrete Coupling Beams Subjected to the Effect of Wind Loading

Sarah Bashour, Bassam Hwaija, and Fadwa Issa

Faculty of Civil Engineering, Tishreen University, Lattakia, Syria

Correspondence should be addressed to Sarah Bashour; sarah.bashour@tishreen.edu.sy

Received 28 February 2023; Revised 25 August 2023; Accepted 4 September 2023; Published 27 September 2023

Academic Editor: Marco Filippo Ferrotto

Reinforced concrete shear walls connected by coupling beams are considered an efficient structural system for tall buildings subjected to lateral loads. For seismic design of such buildings, performance-based design has been commonly used in regions with strong earthquakes for its ability to achieve economical and safe design, however the use of performance-based wind design (PBWD), which permits nonlinear response of ductile elements at specific locations under wind loads is still hindered due to the lack of information regarding the performance of these elements. In addition to that, there is still a need for developing an analytical model that can represent nonlinear behavior of these elements when subjected to wind loads. Therefore, in this study two analytical models using two different methods to consider bond slip effect (Bond SP01 (BS) model and steel modification factor (SMF) model) were developed and implemented in OpenSees software and validated with a tested specimen of reinforced concrete coupling beam subjected to a simulated windstorm loading protocol. Then, a parametric study was conducted using the SMF model to investigate the effect of axial restraint, and modification of the ductility demand. Results showed that both of the models showed good agreement with the experiment, however results of the SMF model were more accurate. As for the parametric study, it was concluded that with axial restraint, the beam behavior was dominated by shear, and a slight increase of strength was observed. At ductility demand of $1.8\theta_y$, the beam performed well with no significant damage and minor residual rotations.

1. Introduction

In shear wall systems subjected to the lateral loads; coupling beams through their inelastic behavior are considered as a reliable source of ductility and energy dissipation. Seismic design in most building permits nonlinear behavior of coupling beams contrary to the wind design which only permits linear behavior of these elements [1].

The current wind design codes often lead to an overestimation of strength and stiffness of the horizontal members such as beams, coupling beams, and braces, and because of that the design requirements of vertical members and joints under the seismic loads would also increase [2].

In recent research, performance-based wind design (PBWD) was introduced and nonlinear behavior of coupling beams has been permitted in buildings subjected to wind loads. However, studies are still in progress in order to investigate whether this limited nonlinearity is acceptable and if coupling beams can be pushed to greater ductility demands without resulting to an unacceptable behavior [1].

There has been many experimental research about performance of coupling beams under the seismic loads but very few under wind loads, Abdullah et al. [1] studied the behavior of reinforced concrete coupling beams with aspect ratios of 2.5 and 3.67 subjected to a wind loading protocol based on the results of nonlinear response history analysis of a coupled core wall system subjected to loading histories taken from a wind tunnel test. They also studied the effect of various parameters such as presence of floor slab and seismic detailing of reinforcement. The beams performed well under wind loads with minor damage, however none of the parameters included in the study had a significant impact on the behavior of the beams and all the tests were done without applying axial load (axial restraint).

In the past few years, analytical modeling has been widely used to study the seismic performance of many structural elements such as coupling beams. According to many

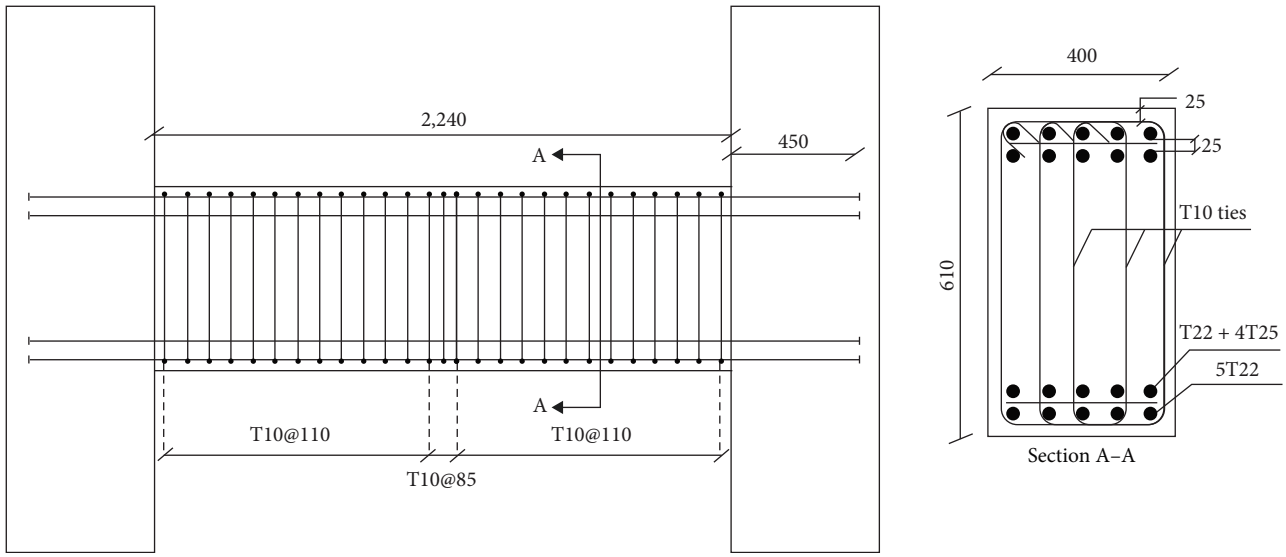

Figure 1: Reinforcement layout and geometry of specimen CB3 [1].

studies, there are four components that contribute to the total deformation of concrete coupling beams which are flexure, bond slip, shear distortion, and shear sliding. Each component's contribution depends on the aspect ratio of the beam and reinforcement layout [1, 3].

Huan et al. [4] performed cyclic analysis on deep conventional coupling beams with aspect ratios ranging from 1 to 3.5 using OpenSees software [5]. The developed model was able to consider the interaction between flexure and shear at the element level. The hysteretic shear model included cracking, yielding, ultimate, and failure as the main four points of its envelope curve, and was implemented in the software using Pinching4 material.

Ding et al. [6] also modeled conventional reinforced coupling beams with aspect ratios from 1 to 4 using MSC.MARC Version 2007r1 software, with more detailed modeling of shear distortion and shear sliding in addition to flexure. The envelope curve of the hysteretic shear force–shear strain model was trilinear with two key feature points: the cracking and the peak point. As for modeling shear sliding, a simplified polyline curve describing the shear force–shear sliding displacement relationship was assigned to an element at the fixed ends of the beam.

However, until this day there has been no development of an analytical model to represent the behavior of these elements when subjected to wind loads.

In this paper, two numerical models (Bond SP01 (BS) model and steel modification factor (SMF) model) of conventional reinforced concrete coupling beams subjected to a wind loading protocol were developed and implemented in the OpenSees software [5]. The experimental program of Abdullah et al. [1] was used for the validation of results.

The two models only differ in bond slip modeling, as for flexure and shear distortion; the same modeling approach is used in both.

A parametric study was then carried out with the use of SMF model in order to investigate the effect of axial restraint and modifying the ductility demand of the wind loading protocol.

2. Experimental Program and Numerical Analysis

2.1. Experimental Coupling Beam Properties and Wind-Loading Protocol. The specimen CB3 from the experimental tests conducted by Abdullah et al. [1] was chosen to validate the numerical model presented in this paper. The length to depth ratio of the coupling beam is 3.67 with standard reinforcement detailing and without floor slab or any axial restraint. The beam was considered to be located in a building in low-seismic hazard area and was designed according to ACI 318-14 [7]. The geometry of the beam and reinforcement layout is illustrated in Figure 1.

The wind loading protocol used in the experimental test was based on a representative wind hazard curve (Figure 2(a)), and the results of a nonlinear response history analysis of a tall coupled core wall building subjected to loading histories recorded from a wind tunnel test (Figure 2(b)) [1].

Developing this protocol firstly involved specifying the amplitude of peak loading cycles by comparing expected demands for a building subjected to a "collapse-level" windstorm with an MRI of approximately 3,000 years to demands from an "infrequent" (but more often occurring) windstorm with an MRI of 100 years using the relationship that wind demands are approximately proportional to the square of the wind speed, then dividing the collapse-level force amplification by the beam overstrength ratio (1.3 or 1.35) which results to the required beam ductility demand. Second, the number and amplitude of cycles before and after the peak cycles were determined by calculating the core wall demands at several stories, then counting and averaging the number of times the demands exceeded several different fractions of the peak demand in the positive and negative directions [1].

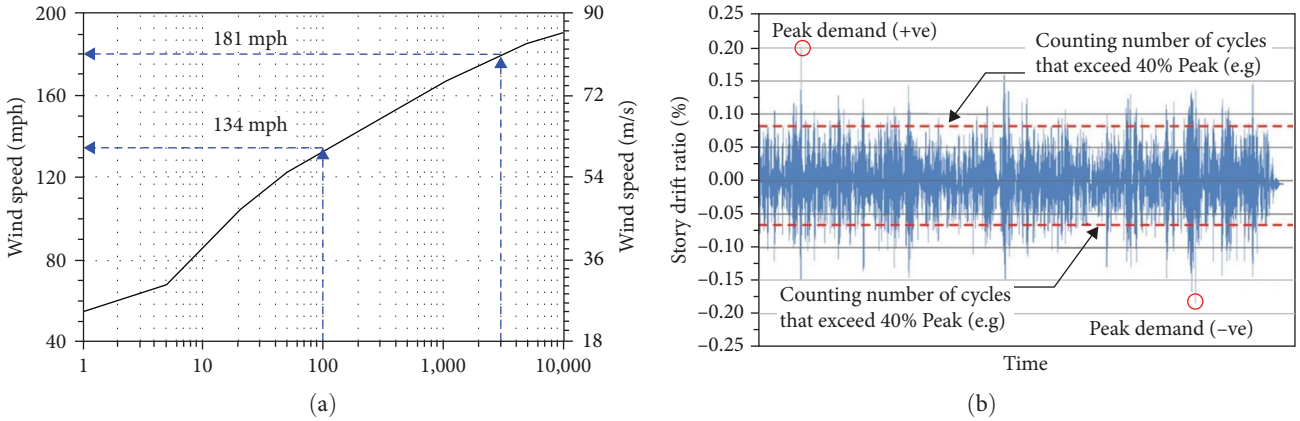

FIGURE 2: Determination of wind loading protocol. (a) Representative wind hazard curve for Miami, FL, created with historical and hurricane simulation data. (b) Example demand of core wall subjected to time histories recorded from wind tunnel tests [1].

The developed protocol consists of first three stages which are applied as force controlled (ramping up from 15% to 75% of the probable moment strength (M_{pr}), then displacement controlled for another three stages (1.2 then 1.5 followed by another 1.2 time the yield rotation (θ_y) to go back to a three stages of force control. The details of the protocol are shown in Figure 3(a). As for the test setup, a horizontal hydraulic actuator was used to apply the lateral load using a steel loading beam, and two vertical hydraulic actuators were used to ensure a double-curvature loading condition. No axial load (or axial restraint) was applied. To prevent out-of-plane rotation, the steel loading beam was connected to two out-of-plane actuators, which were attached to steel reaction braced frames. the details of the test setup implementation are illustrated in Figure 3(b) [1].

2.2. Bond SP01 (BS) Model

2.2.1. Overall Finite Element Model. The first model used in this study consists of one nonlinear beam column element with 10 integration points. The two rigid blocks on both sides of the beam were modeled using elastic beam column elements with large stiffnesses. The used fiber section consists of a confined concrete core, unconfined concrete cover, and steel rebars, their constitutive models are detailed in Section 2.2.2. To account for bond slip effects, a zero-length section element was added to each end of the nonlinear beam column element, where a modified concrete model is used and the material used for steel fibers is Bond SP01. The zero-length section element is furtherly discussed in Section 2.2.4, and the details of the model are shown in Figure 4.

2.2.2. Constitutive Models of Concrete and Steel Rebars. (*1*) *Concrete Material.* There are many reported models of concrete's behavior in the literature. For the confined concrete core, Mander et al.'s [8] model illustrated in Figure 5 is used for compression. The unconfined compressive strength f'_{co} and the corresponding strain ε'_{co} as well as the young modulus E_c is taken from the experimental tests. The tensile strength of concrete is taken as $f_t = 0.62\sqrt{f'_c}$ [9]. The model was implemented in OpenSees by the available uniaxial material Concrete 02 [5] shown in Figure 6(a).

For the unconfined concrete cover, Kent and Park model [10] with zero tensile strength is used. The model is known as concrete 01 in OpenSees [5] and is shown in Figure 6(b).

(*2*) *Steel Material.* For modeling steel rebars, uniaxial material hysteretic illustrated in Figure 7 is used [5]. The yield, ultimate, and rupture strength $(f_{sy}, f_{su}, f_{srup})$ as well as their corresponding strains $(\varepsilon_{sy}, \varepsilon_{su}, \varepsilon_{srup})$ of the rebars were also taken from the experimental tests.

Defining the hysteretic behavior of the previous material includes: pinching parameters (*pinchx*, *pinchy*), damage parameters (*damage* 1, *damage* 2), and parameter *beta* to determine the degraded unloading stiffness based on ductility. These parameters were specified by calibrating experimental results, and their values are shown in Table 1.

2.2.3. Shear Model. A trilinear backbone curve describing the force–strain relationship on section level is proposed to model shear behavior of conventional intermediate length coupling beams, the material *hysteretic* is used to represent the relationship and is aggregated with the fiber section using the command *section aggregator*. As shown in Figure 8, three main points are defined on the curve: the cracking point (V_{cr}, γ_{cr}), the peak point (V_{us}, γ_{us}), and the failure point (V_f, γ_f).

The values of V_{cr} and V_{us} are taken as shown in Equations (1) and (2) [6], as for V_f the value $0.2V_{us}$ is recommended [4].

Nabilah and Koh [11] found that before the cracking point, the initial shear stiffness ($K_s = G.A_g/1.2$) for intermediate coupling beams reduces to approximately $0.2K_s$ at the first diagonal crack, therefore γ_{cr} is computed by Equation (3). As for γ_{us}, Equation (4) proposed by Gong and Fang [12] to compute the peak shear strain is used. Finally, the stiffness of the descending branch is taken as $0.001K_s$ [6].

$$V_{cr} = \left(0.158\sqrt{f_c'} + 17.2\rho_{sv}d/a\right)bd \le 0.29\sqrt{f_c'}bd\,, \tag{1}$$

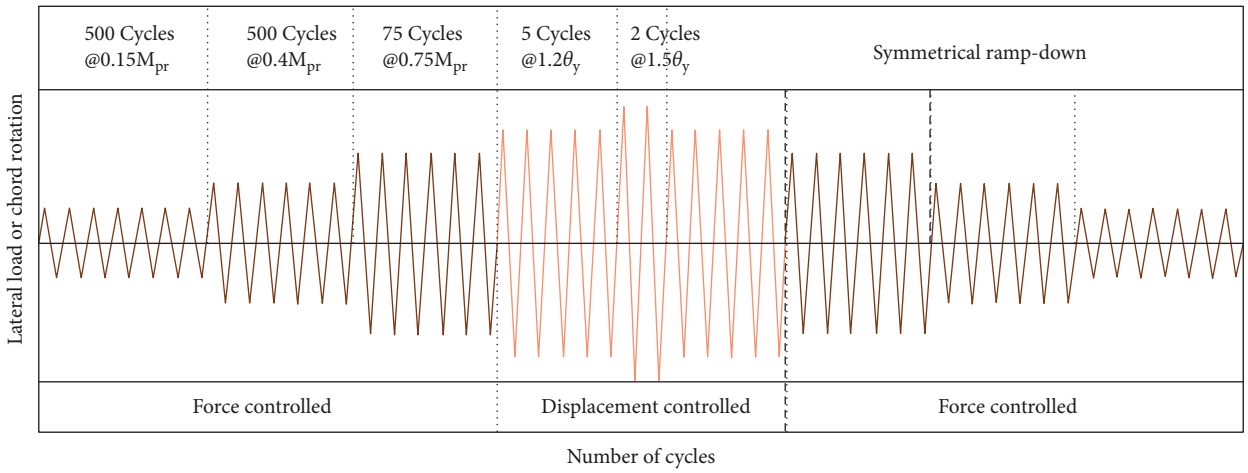

(a)

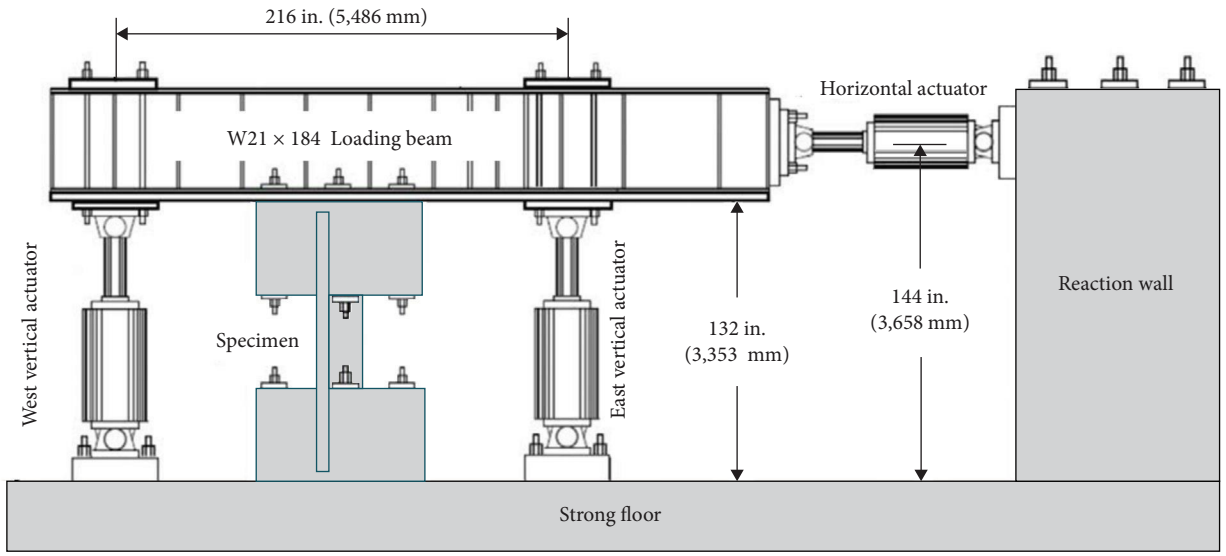

(b)

FIGURE 3: Details of the wind loading test: (a) wind loading protocol and (b) test setup [1].

$$V_{us} = \frac{A_{sv} f_{sv} d}{s} + 0.166\sqrt{f_c'}\, bd\,, \tag{2}$$

$$\gamma_{cr} = \frac{V_{cr}}{0.2K_s}\,, \tag{3}$$

$$\gamma_{us} = \frac{V_{us}}{0.65GA_g}\left[\frac{7l}{h} - 0.73\left(\frac{l}{h}\right)^3\right], \tag{4}$$

where b, h, and d: width, height and effective height of the section, respectively, a: shear span = half of the length l, A_g: area of the section, $A_{sv}, f_{sv}, s, \rho_{sv}$: area, yield stress, spacing, and ratio of transverse reinforcement, respectively, where $\rho_{sv} = A_{sv}/b.s$, f_c': cylinder concrete compressive strength, G: concrete shear modulus $= 0.4E_c$, where E: concrete elastic modulus, K_{ini}: initial section shear stiffness, K_{cr}: section shear stiffness after diagonal cracking, K_{deg}: slope of descending branch.

2.2.4. Bond Slip Model. To consider the bond slip effect between rebars and the surrounding concrete in the BS model, two-zero length section elements were implemented at the ends of the beam column element. A zero-length section element is a fiber discretization of the cross-section of a structural member, and has the ability to incorporate the fixed-end rotation caused by strain penetration to the beam column element, because a zero-length section element is assumed to have a unit length such that the element deformation (for example, rotation) would be equal to the section deformation (for example, curvature) [13].

The materials used in the fiber section of these elements for core and cover concrete are the same as the fiber section of the beam column element but with different inputs as will be discussed later. The hysteretic material Bond SP01 developed by Zhao and Sritharan [13] is applied to describe the cyclic response of steel. The details of the model are illustrated in Figure 9.

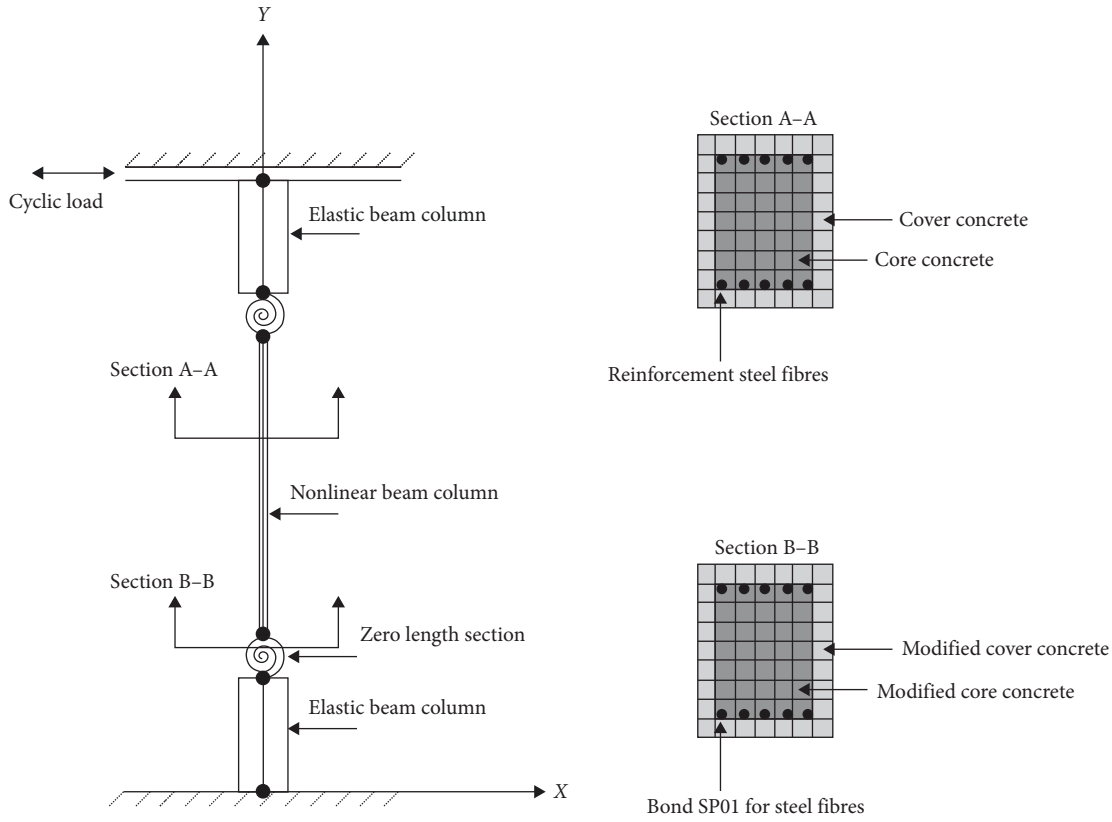

Figure 4: Schematic details BS model.

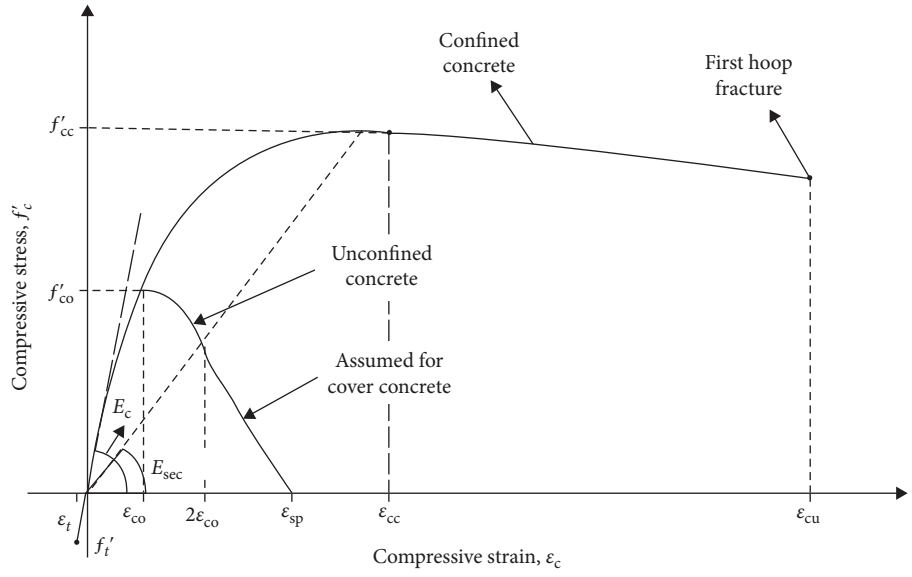

Figure 5: Mander model for confined concrete in compression [8].

The yield and ultimate stress hold the same values as those of the steel rebars in the beam element fiber section. However, the corresponding slip values were calculated using Equations (5) –(15) recommended by Naish et al. [14] as follows:

$$l_d = \frac{440 \times A_b}{K \times \sqrt{f_c'}} \frac{f_{sy}}{400} [\text{mm}], \quad (5)$$

where $K = 3.\text{d}_\text{b}$

$$u_e = \frac{f_{sy} \times d_b}{4 \times l_d} [\text{MPa}], \quad (6)$$

$$L_e = \frac{f_s \times d_b}{4 \times u_e} [\text{mm}], \quad (7)$$

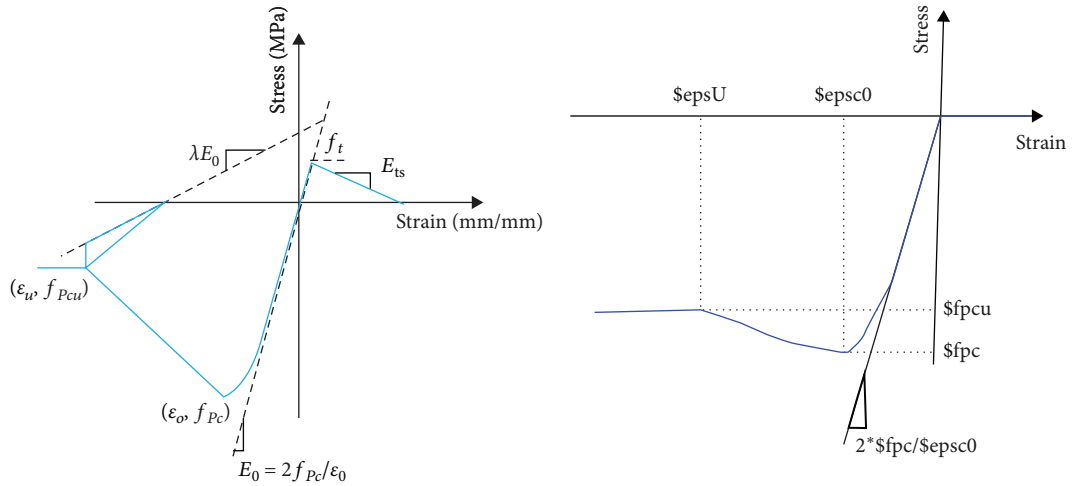

Figure 6: Concrete materials used in the fiber section: (a) Concrete 02 for core and (b) Concrete 01 for cover [5].

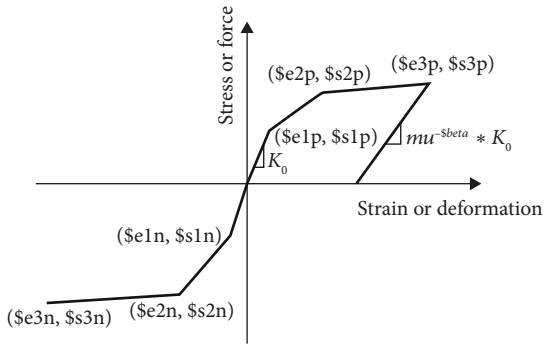

Figure 7: Hysteretic material used for modeling steel rebars [5].

$$u_u = \left(20 - \frac{d_b}{4}\right) \times \sqrt{\frac{f_c'}{30}}[\text{MPa}], \tag{8}$$

$$\delta_{s1} = \sqrt{\frac{30}{f_c'}}[\text{mm}]. \tag{9}$$

When $f_s = f_{sy}$

$$\delta_s = \delta_{s1} \times \left(\frac{u_e}{u_u}\right)^{2.5}[\text{mm}], \tag{10}$$

$$\delta_{exty} = 1.25 \times \varepsilon_{sy} \times \frac{L_e}{2}[\text{mm}], \tag{11}$$

$$S_y = \delta_{toty} = \delta_s + \delta_{exty}[\text{mm}]. \tag{12}$$

When $\varepsilon_s = \varepsilon_{su}$

$$u_f = \left(5.5 - 0.07 \times \frac{S_L}{H_L}\right) \times \sqrt{\frac{f_c'}{27.6}}[\text{MPa}], \tag{13}$$

Table 1: Temperature and wildlife count in the three areas covered by the study.

Parameter	Pinch x	Pinch y	Damage 1	Damage 2	Beta
Value	0.45	0.12	0.0	0.0	0.5

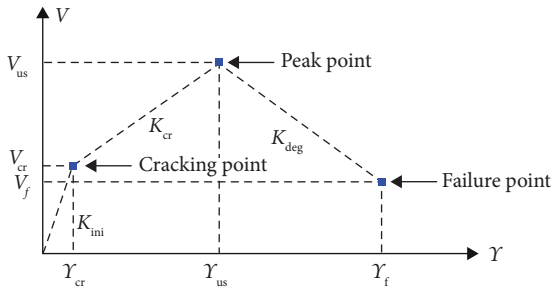

Figure 8: Shear force–shear strain backbone curve.

$$L_{py} = \frac{\Delta f_s \times d_b}{4 \times u_f}[\text{mm}], \tag{14}$$

$$S_u = \delta_{\text{ext}} = \delta_{\text{exty}} + \frac{(\varepsilon_{\text{sy}} + \varepsilon_{\text{su}}) \times L_{py}}{2}[\text{mm}]. \tag{15}$$

Further improvement of Zhao and Sritharan [13] method was suggested by Ghannoum [15]. A modification factor r_y computed using Equation (16) is used to scale the material strain in the bar-slip element (zero length section element), which was used to modify the input data of concrete. Further details of the method's implementation are explained in the previous studies [15, 16].

$$r_y = \frac{E_s}{E_{\text{slip}}} = \frac{S_y}{\varepsilon_{\text{sy}}} E_{\text{slip}} = \frac{f_{\text{sy}}}{S_y}. \tag{16}$$

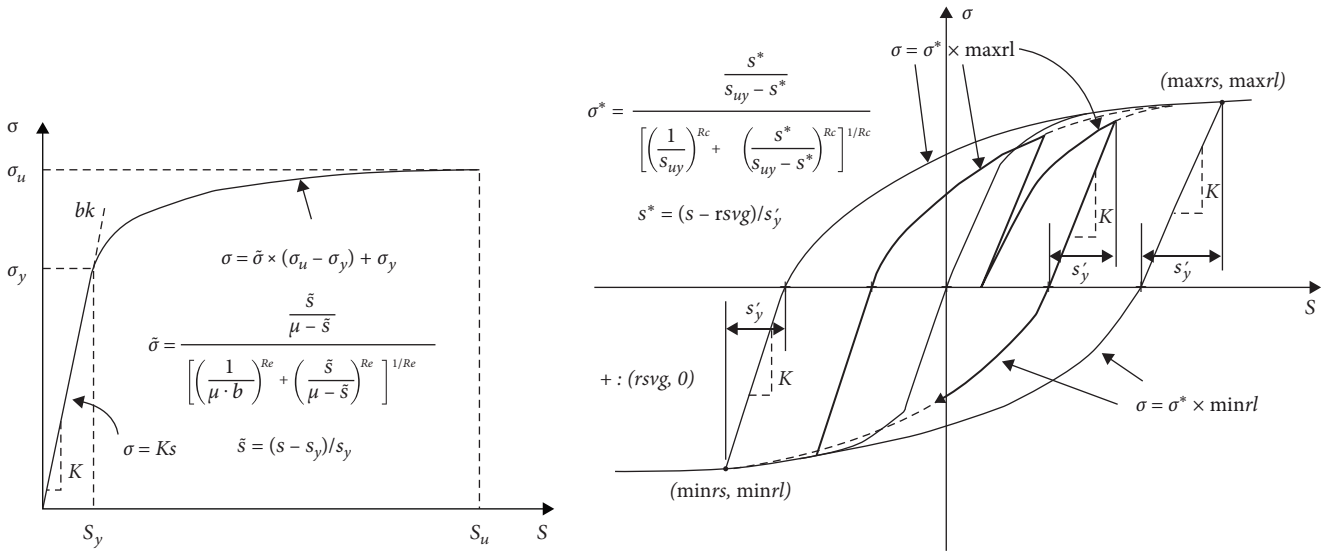

FIGURE 9: Bond SP01 model proposed by Zhao and Sritharan [13].

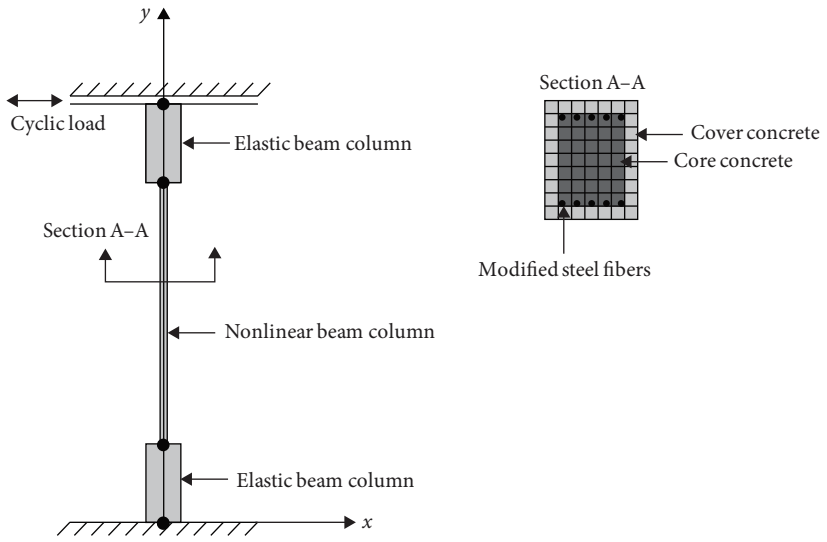

FIGURE 10: Schematic details SMF model.

Where E_s : Young's modulus of steel, f_{sy} : yield stress of steel, ε_{sy} : strain at yield of steel, and S_y : amount of slip of steel out of anchorage at yield stress.

2.3. Steel Modification Factor (SMF) Model. The SMF model is the same as the previous BS model except for the bond slip effect. As it is shown in Figure 10, there is no need for a zero-length section element at the ends of the beam column element which was needed in the previous model. Other details such as materials and the shear model remain the same.

In order to consider the bond slip effect, the method proposed by Sharifi et al. [17] is used. The developed method modifies the rebar elastic modulus E_s by a modification coefficient λ determined by Equation (17).

$$\lambda = \frac{\varepsilon_{sy}}{\varepsilon_s + \varepsilon_b}, \tag{17}$$

where ε_{sy} is the yield strain of steel, ε_b is the equivalent bond–slip strain taken as Equation (18).

$$\varepsilon_b = \frac{S_{yeild}}{L_p}, \tag{18}$$

where S_{yeild} is the maximum slip value for yield rebar stress computed using Equation (19). L_p is the equivalent plastic hinge length approximated by Equation (20) which is proposed by Priestley et al. [18].

$$S_{yeild} = \left[\frac{(1+\alpha_b) d_b S_1^{\alpha_b}}{8(1+n\rho_e) E_s \tau_{b\max}} f_y^2\right]^{\frac{1}{1+\alpha_b}}, \tag{19}$$

where the values of $\alpha_b, \tau_{b\max}, S_1$ can be taken from CEB-FIP [19].

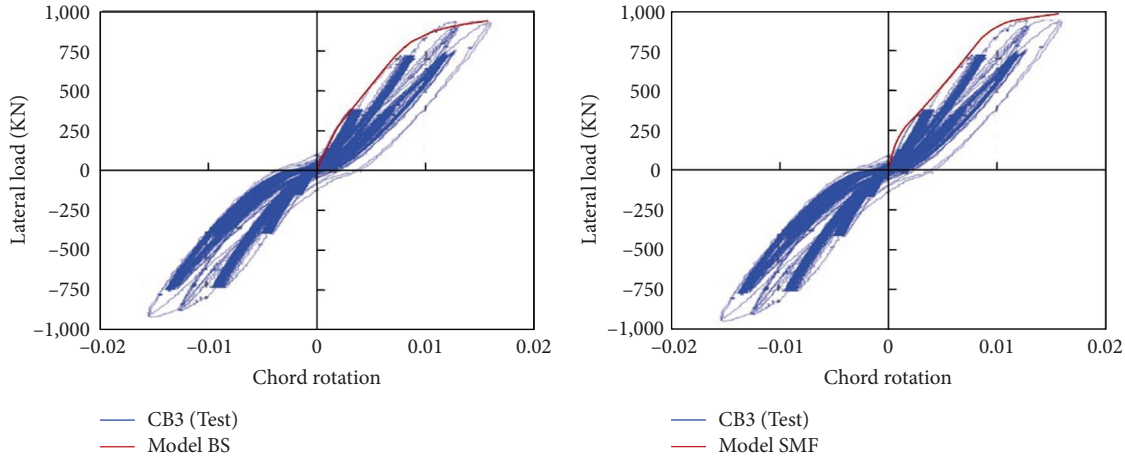

Figure 11: Comparison of the pushover curves of both models with the experimental hysteretic behavior: (a) bond SP01 model and (b) steel modification factor model.

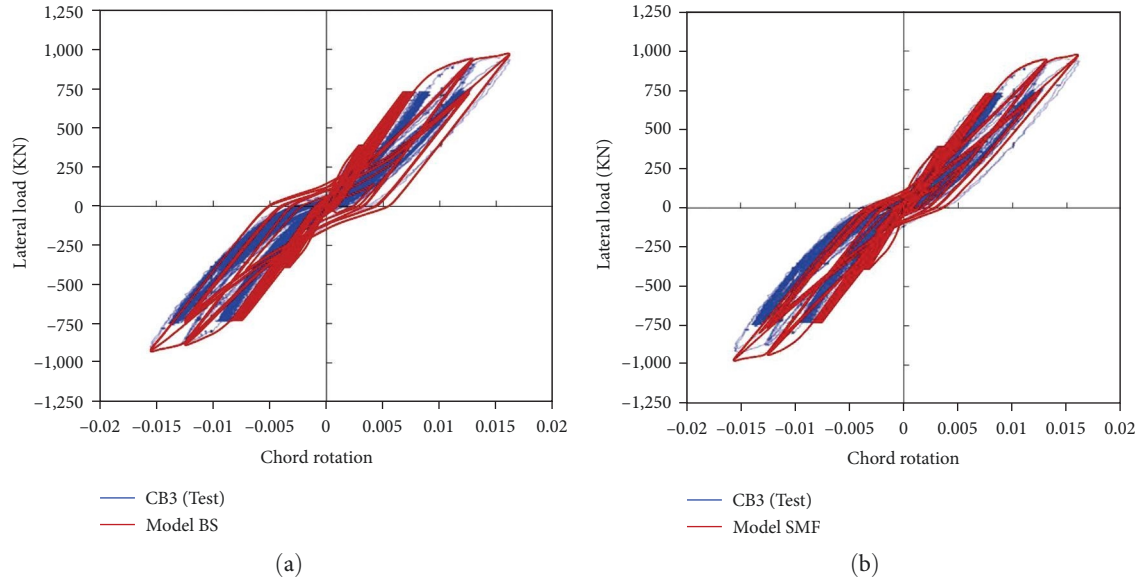

Figure 12: Comparison of the hysteretic curves of both models with the experimental one: (a) bond SP01 model and (b) steel modification factor model.

$$L_p = 0.2\left(\frac{f_{su}}{f_{sy}} - 1\right)L_c \leq 0.08L_c\,, \tag{20}$$

where f_{sy} is the rebar yield strength, f_{su} is the rebar ultimate strength, and L_c is the length from the maximum moment section to the moment diagram's inflexion point.

3. Analysis Results and Discussions

3.1. Pushover Analysis Results. A pushover analysis was first conducted for both models as shown in Figure 11. Results were compared with the corresponding backbone curve taken from the experiment. Figures 11(a) and 11(b) show that the initial stiffness of the pushover curves for both models is very close to the experimental one. However, in the nonlinear part, a slight difference is observed in the SMF model. As can be seen the maximum strength in BS model reached 940 KN compared to 954 KN from the experiment with a difference of 1.46%. However, for SMF model the value reached 977 KN with a difference of 2.4%.

3.2. Cyclic Wind Loading Analysis Results. The cyclic wind loading protocol described in Section 2.1 was applied. For this study, the first six stages of the protocol were fully applied just like the experiment. However, for the last three stages only one cycle of each peak was applied as displacement controlled in the negative and positive direction. Figure 12 shows the hysteretic response of the numerical analysis compared to the experimental results.

Both of the models gave good results in predicting the backbone curve, including various important characteristics. First, the chord rotation values corresponding to the last

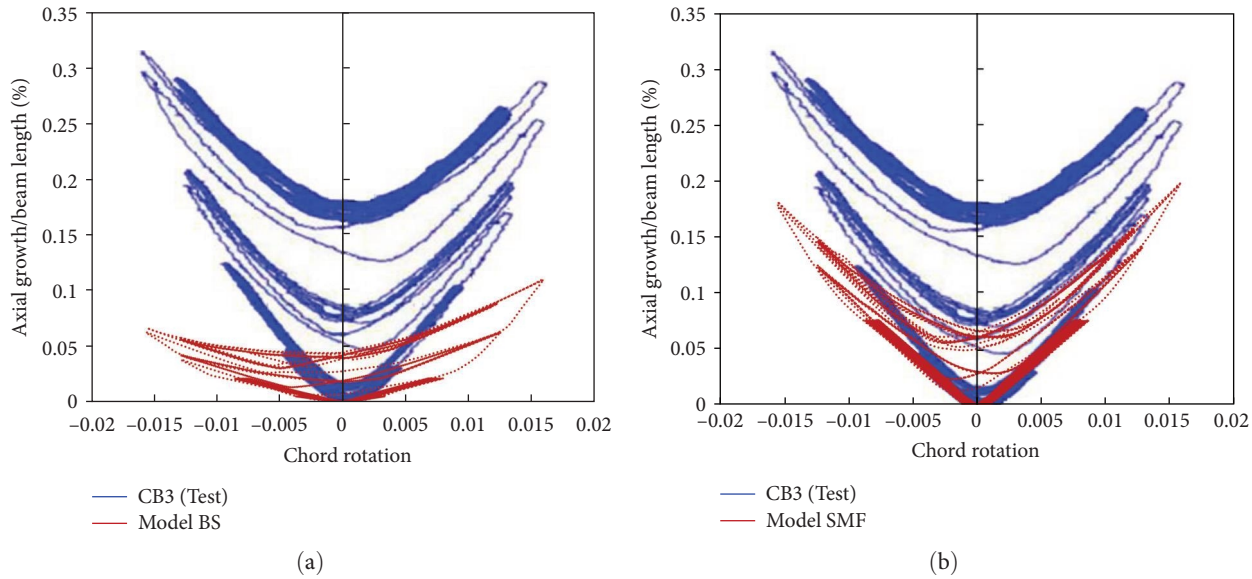

Figure 13: Comparison of the axial growth versus chord rotation of both models with the experimental one: (a) bond SP01 model and (b) steel modification factor model.

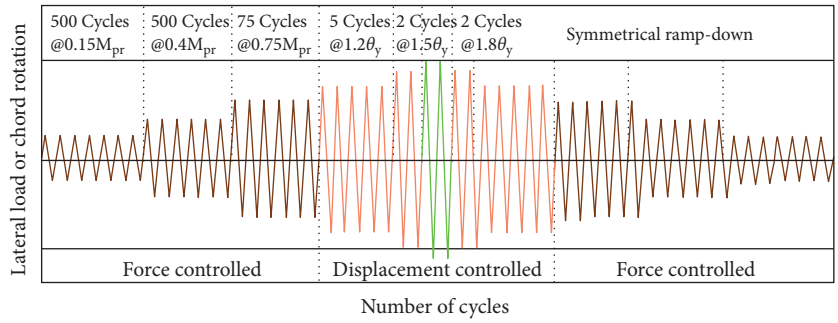

Figure 14: The modified loading protocol.

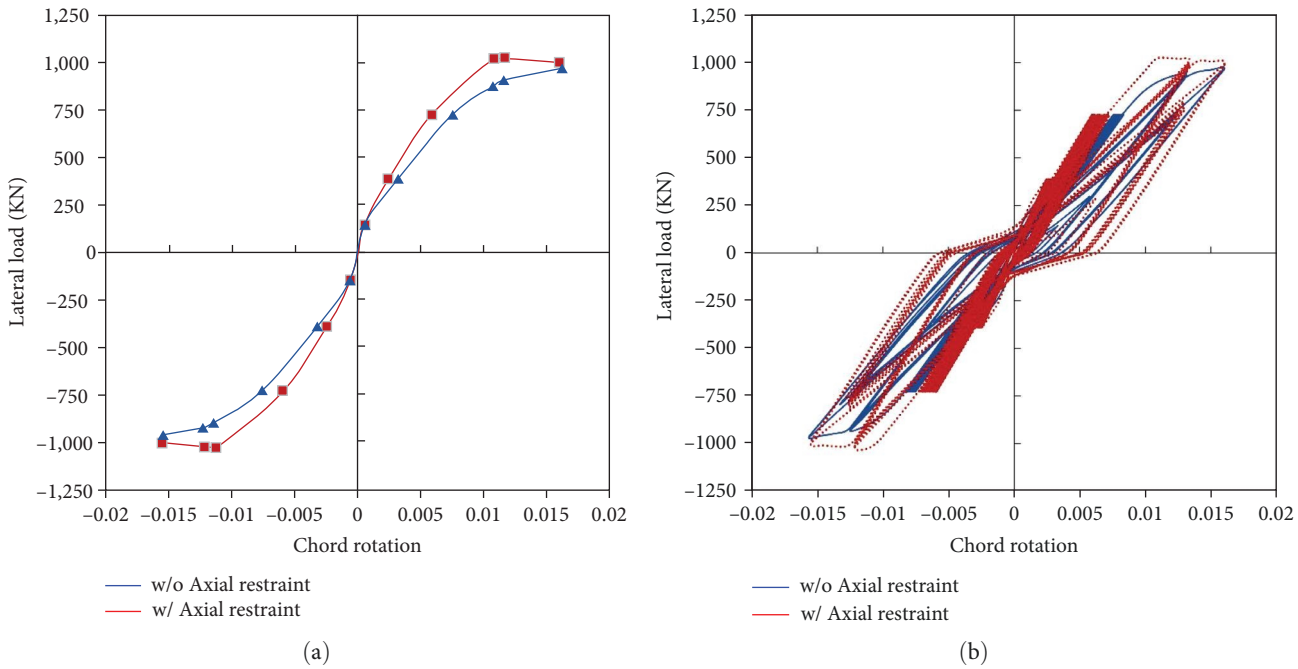

Figure 15: Effect of axial restraint on the behavior of the coupling beam: (a) backbone curves and (b) hysteresis curves.

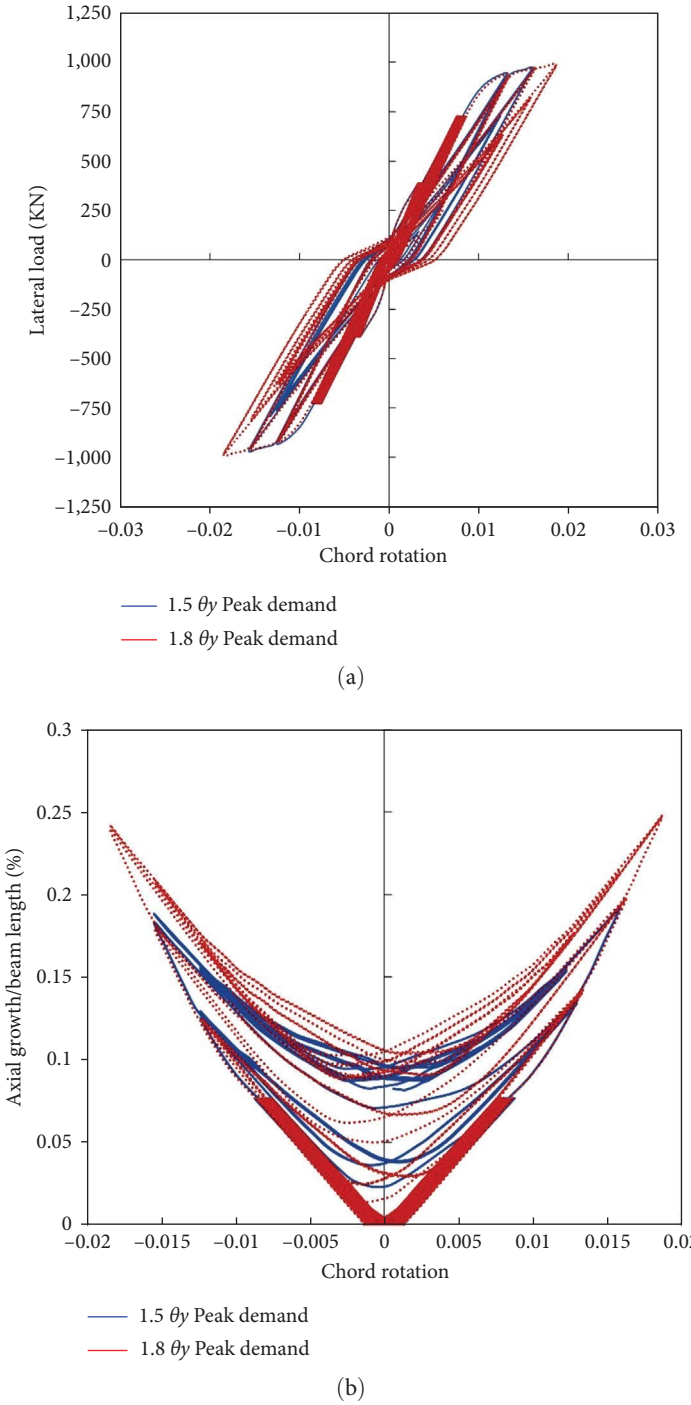

Figure 16: Effect of modifying ductility demand on the behavior of the coupling beam: (a) hysteresis curves and (b) axial growth versus chord rotation curves.

cycle of $0.75M_{pr}$ in the positive and negative direction, respectively, were underestimated by approximately 9.5% and 8.7% for the BS model and 2.3% and 9.3% for the SMF model. Second, for the strength corresponding to the second cycle of $1.5\theta_y$, both models matched well with the results with a difference of 1.05% and 0.65% for the BS model and 1.26% and 4.36% for the SMF model. SMF model was also able to predict residual rotations and model pinching behavior which appears notably in the case of wind loads, showing much better results than BS model.

As shown in Figure 13, the relation between axial growth and chord rotation was also compared with the experimental ones. Figure 13(a) shows the results of the BS model where the percentage of the maximum axial growth to beam length is greatly underestimated by approximately 76% in comparison with the test. As for the SMF

model, Figure 13(b) shows much better results with a difference of about 36%.

It can be concluded from the previous comparisons that both of the models showed overall good results. However, the SMF model can predict with more accuracy the hysteretic behavior of reinforced concrete coupling beams subjected to wind loads, therefore it is more suited for use in the parametric studies related to concrete coupling beams.

4. Parametric Study

4.1. Parameters Included in the Study. The proposed SMF model mentioned above was used to conduct a parametric study on the behavior of coupling beams subjected to wind loads. Two parameters including axial restraint and modifying peak ductility demand were taken into account.

In general, coupling beams in coupled wall systems are not free to elongate as there is a level of axial restraint applied from the adjacent walls. The axial force corresponding to this restraint is expected to affect the strength of the coupling beam and its general behavior hence the possibility of altering the behavior of the coupled wall by preventing yielding in the coupling beams and transferring larger axial forces into the walls [20]. Therefore, a full axial restraint is applied in this study to investigate its effect on the behavior of the coupling beam subjected to wind loads.

In addition to that, experimental results from Abdullah et al. [1] showed that the tested coupling beams performed well with minor damage and it was suggested that if they were to be pushed to a greater ductility demand they would reach higher lateral strengths. Therefore, two cycles of a ductility demand equal to $1.8\theta_y$ is applied in this section followed by two cycles of $1.5\theta_y$ to achieve symmetry. For the rest of the cycles, they remain the same as before as shown in Figure 14.

4.2. Results and Discussions of the Parametric Study

4.2.1. Effect of Axial Restraint. Figure 15 illustrates the effect of axial restraint on the behavior of the coupling beam subjected to wind loads. As can be seen from the backbone curves in Figure 15(a) with axial restraint, a slight increase in initial stiffness and strength can be observed indicating an improvement of the beam's moment resistance due to the axial force. The maximum strength of 1,024 KN was recorded at a chord rotation of $1.11\theta_y$ with an increase of about 13% in comparison with no axial restraint. However, after this value the strength of the beam begins to decrease until it reaches a value of 1,000 versus 969 KN for the case of no axial restraint with a minor difference of about 3% at rotation $1.5\theta_y$. This may be the result of the shear force at probable moment $V_{@Mpr}$ being greater than the nominal shear strength V_N, and thus resulting of shear dominating the behavior of the beam.

From Figure 15(b), it can be seen that with axial restraint, the pinching behavior was slightly less and the residual rotations increased to reach approximately 0.0058. Lastly, a slight increase of post peak strength degradation has occurred.

4.2.2. Effect of Modifying the Ductility Demand. As expected, it can be seen from Figure 16(a) that the strength of the beam at the peak ductility demand of $1.8\theta_y$ reached a higher value of 986 KN due to strain hardening of longitudinal reinforcement. As for the last cycle of chord rotation $1.2\theta_y$ in the ramp down, the strength of the beam decreased to approximately 620 versus 740 KN for the case of maximum ductility of $1.5\theta_y$ with a difference of 15%.

Residual chord rotations reached a value of 0.005 which was considered neglectable in Abdullah et al. [1].

From Figure 16(b), it can be observed that the maximum axial growth was 0.24 at ductility demand of $1.8\theta_y$, and a very small change was observed in the cycles of the ramp down.

Just like the ductility demand of $1.5\theta_y$ in the tests of Abdullah et al. [1], almost all of the axial growth takes place before the maximum demand with no axial growth after it, indicating that no new cracks formed in the ramp down cycles.

From the results above it be can concluded that for conventional reinforced concrete coupling beams, a ductility demand of $1.8\theta_y$ was achieved with no significant damage observed and minor residual rotations.

5. Conclusions

In this paper, two numerical models of conventional reinforced concrete coupling beams subjected to a wind loading protocol were implemented and validated with experimental results. Then a parametric study was conducted to investigate the effect of axial restraint and modifying the ductility demand.

Based on the results of this research, the following conclusions can be made:

(1) The proposed models in this study: the first including zero length section element at the ends of the beam with Bond SP01 to model steel (model BS), and the second using a modification steel factor (model SMF), produced pushover curves and an overall hysteretic behavior that matched well with the experimental results. The models differed only in modeling bond slip effect and used the same modeling approach for flexure and shear.

(2) SMF model showed better results in predicting pinching behavior, residual rotations, and axial growth of the beams than model BS and therefore was deemed more adequate for use in parametric studies.

(3) With axial restraint, the behavior of the beam was dominated by shear. An increase of post peak strength degradation as well as a slight increase in strength was observed. The increase of strength reached a maximum value of about 13% at rotation $1.11\theta_y$, and a minimum of 3% only at rotation $1.5\theta_y$.

(4) A ductility demand of $1.8\theta_y$ can be achieved with minor residual rotations and no significant damage in conventional reinforced concrete coupling beams subjected to wind loads.

Nomenclature and Notation

a: Shear span
A_b: Area of longitudinal bar
A_g: Area of the section
A_{sv}: Area of transverse reinforcement
b: Width of the section
BS: Bond SP01
d: Effective height of the section
d_b: Diameter of longitudinal bar
h: Height of the section
H_L: Height of the lugs on the reinforcement
$E_c = E_o$: Modulus of elasticity of concrete
E_s: Modulus of elasticity of steel
E_{sec}: Secant modulus of confined concrete at peak stress
$f_c^{'} = f_{co}^{'}$: Compressive strength of unconfined concrete
$f_{cc}^{'}$: Compressive strength of confined concrete
f_{pc}: Compressive strength of concrete at 28 days
f_{pcu}: Ultimate compressive strength of concrete at 28 days
f_{srup}: Rupture stress of steel
f_{su}: Ultimate stress of steel
f_{sv}: Yield stress of transverse reinforcement
f_{sy}: Yield stress of steel
f_t: Tensile strength of concrete
G: Shear modulus of concrete
K_s: Uncracked shear stiffness
K_{ini}: Initial section shear stiffness
K_{cr}: Section shear stiffness after diagonal cracking
K_{deg}: Slope of descending branch
l: Length of the beam
L_c: The length from maximum moment section to moment diagram's inflection point
l_d: Development length
L_e: Elastic region length
L_p: Equivalent plastic hinge length
L_{py}: Post yield length
M_{pr}: Probable moment strength
MRI: Mean recurrence interval
PBWD: Performance-based wind design
r_y: Modification factor used to scale the material strain in the bar slip element
s: Spacing of transverse reinforcement
S_L: Spacing of the lugs on the reinforcement
S_u: Rebar slip at member interface at the bar fracture strength
S_y: Rebar slip at member interface under yield stress
S_{yield}: Maximum slip value for yield rebar stress
S_1: Slip when peak value of bond stress is obtained
SMF: Steel modification factor
u_e: Elastic bond stress
u_u: Peak bond stress
$V_{@Mpr}$: Shear strength at probable moment
V_{cr}: Cracking shear force
V_f: Shear force at failure
V_n: Nominal shear strength
V_{us}: Peak shear force
α_b: Exponential factor
γ_{cr}: Cracking shear strain
γ_f: Shear strain at failure
γ_{us}: Peak shear strain
δ_{ext}: Extension of the bar due to accumulation of strain along its length
δ_s: Slip of the reinforcement
δ_{s1}: Local slip at peak bond stress
δ_{tot}: Total displacement of the bar at the beam-wall interface
ε_b: Equivalent bond slip strain
$\varepsilon_{co} = $ epsco: Strain at maximum stress f'_{co} of unconfined concrete
$\varepsilon_{cc} = \varepsilon_o$: Strain at maximum stress f'_{cc}
$\varepsilon_{cu} = \varepsilon_u$: Ultimate concrete compressive strain
ε_{srup}: Rupture strain of steel
ε_{su}: Ultimate strain of steel
ε_{sy}: Yield strain of steel
θ_y: Yield rotation
λ: Modification coefficient of rebar elastic modulus
ρ_{sv}: Ratio of transverse reinforcement
τ_{bmax}: Peak value of bond stress.

Data Availability

The data used to support the findings of this study are included within the article.

Conflicts of Interest

The authors declare that there are no conflicts of interest.

Acknowledgments

This research work was supported by Tishreen University.

References

[1] S. A. Abdullah, K. Aswegan, S. Jaberansari, R. Klemencic, and J. W. Wallace, "Performance of reinforced concrete coupling beams subjected to simulated wind loading," *ACI Structural Journal*, vol. 117, no. 3, pp. 283–295, 2020.

[2] S. Y. Jeong, H. Alinejad, and T. H.-K. Kang, "Performance-based wind design of high-rise buildings using generated time-history wind loads," *Journal of Structural Engineering*, vol. 147, no. 9, Article ID 04021134, 2021.

[3] S. F. Breña and O. Ihtiyar, "Performance of conventionally reinforced coupling beams subjected to cyclic loading," *Journal of Structural Engineering*, vol. 137, no. 6, pp. 665–676, 2011.

[4] L. Huan, D. Ke, S. Jing-jiang, and D. Bao-rong, "Hysteretic shear and analysis models for reinforced concrete coupling beams with small span-to-depth ratios," *Engineering Mechanics*, vol. 35, no. 9, pp. 161–169, 179, 2018.

[5] F. McKenna, G. L. Fenves, and M. H. Scott, *Open System for Earthquake Engineering Simulation*, University of California, Berkeley, 2000.

[6] R. Ding, M.-X. Tao, J.-G. Nie, and Y. L. Mo, "Shear deformation and sliding-based fiber beam–column model for seismic analysis of reinforced concrete coupling beams," *Journal of Structural Engineering*, vol. 142, no. 7, Article ID 04016032, 2016.
[7] ACI 318-14, *Building Code Requirements for Structural Concrete: CCOMMENTARY on Building Code Requirements for Structural Concrete (ACI 318R-14)*, American Concrete Institute, Farmington Hills, MI, 2014.
[8] J. B. Mander, M. J. N. Priestley, and R. Park, "Theoretical stress–strain model for confined concrete," *Journal of Structural Engineering*, vol. 114, no. 8, pp. 1804–1826, 1988.
[9] ACI 318-19, *Building Code Requirements for Structural Concrete: CCOMMENTARY on Building Code Requirements for Structural Concrete (ACI 318R-19)*, American Concrete Institute, Farmington Hills, MI, 2019.
[10] D. C. Kent and R. Park, "Flexural members with confined concrete," *Journal of the Structural Division*, vol. 97, no. 7, pp. 1969–1990, 1971.
[11] A. B. Nabilah and C. G. Koh, "Experimental study of intermediate length coupling beams subjected to monotonic load," *KSCE Journal of Civil Engineering*, vol. 21, pp. 2807–2813, 2017.
[12] B. N. Gong and E. H. Fang, "Experimental investigation and full range analysis of reinforced concrete coupling beams between shear walls," *Building Science*, vol. 4, no. 4, pp. 39–43, (In Chinese), 1988.
[13] J. Zhao and S. Sritharan, "Modeling of strain penetration effects in fiber-based analysis of reinforced concrete structures," *ACI Structural Journal*, vol. 104, no. 2, pp. 133–141, 2007.
[14] D. Naish, A. Fry, R. Klemencic, and J. Wallace, "Reinforced concrete coupling Beams—Part II: modeling," *ACI Structural Journal*, vol. 110, no. 6, pp. 1067–1075, 2013.
[15] W. M. Ghannoum, *Experimental and Analytical Dynamic Collapse Study of a Reinforced Concrete Frame with Light Transverse Reinforcement*, Doctoral Dissertation, University of California, Berkeley, 2007.
[16] D. V. To, *Performance Characterization of Beams with High-Strength Reinforcement*, Doctoral Dissertation, University of California, Berkeley, 2018.
[17] A. Sharifi, M. R. Banan, and M. R. Banan, "A macro-method for including bond–slip flexibility within fibre element formulation for simulating hysteretic behaviour of RC beam–column members," *Iranian Journal of Science and Technology, Transactions of Civil Engineering*, vol. 44, pp. 631–643, 2020.
[18] M. J. N. Priestley, G. M. Calvi, and M. J. Kowalsky, *Displacement-Based Seismic Design of Structures*, IUSS PRESS, Pavia Italy, 2007.
[19] CEB-FIP, *Bond of Reinforcement in Concrete*, Fib CEB-FIP, 2000.
[20] B. A. B. Al-Khateeb, *Experimental Study of Reinforced Concrete Coupling Beams with Axial Restraint*, Master Thesis, Washington State University ProQuest Dissertations Publishing, 2021.